Self-Assembly Behavior of AB/AC Diblock Copolymer Mixtures in Dilute Solution

Ying Zhuang, Jiaping Lin,* Liquan Wang, and Liangshun Zhang

Key Laboratory for Ultrafine Materials of Ministry of Education, School of Materials Science and Engineering, East China University of Science and Technology, Shanghai 200237, China

Received: October 16, 2008; Revised Manuscript Received: December 7, 2008

The self-assembly behavior of AB/AC amphiphilic diblock copolymer mixtures in dilute solution was studied by a real-space-implemented self-consistent field theory in three dimensions. The AB and AC copolymers have a common hydrophobic block A but different hydrophilic blocks B and C. Two cases were studied: one in which copolymers AB and AC have same hydrophobic and hydrophilic block lengths and one in which copolymers AB and AC have different hydrophobic and hydrophilic block lengths. It was found that the two copolymers can cooperatively self-assemble into hybrid aggregates. The morphologies of the formed aggregates were found to be dependent on the mixture ratio and the interaction between the B and C blocks. For the AB/AC copolymers with different hydrophobic and hydrophilic lengths, chain segregation was found in the formed hybrid aggregates. Based on the obtained calculation results, phase diagrams as functions of the mixture ratio and interaction between the B and C blocks were constructed.

Introduction

The capability of amphiphilic copolymers to self-assemble into nanoscale microstructures in dilute solution has attracted widespread interest because of their applications in drug delivery, the cosmetics industry, and encapsulation technologies.[1−12] The application of microstructure aggregates mainly depends on the properties of their cores and shells. By altering the structure and composition of the core and shell, many new properties can be produced to broaden the range of potential applications and to fabricate novel types of aggregates with special and controllable structures. Compared to the design and synthesis of a new copolymer with novel microstructures, cooperative self-assembly of two different copolymers to manipulate the structures is an efficient approach. The aggregate structures can be easily tuned by variation of properties of the mixed system such as the mixture ratio and interaction parameters. The hybrid aggregates with tunable structures can exhibit unique properties and are capable of meeting various requirements in applications.[13−17] For example, we have prepared a kind of hybrid micelle from polypeptide block and graft copolymer mixtures and examined their drug carrier capability.[16] We found that the drug release rate was dependent on the mixed ratio of the two copolymers. This provides an easy way to control the drug delivery behavior.

Regarding the cooperative self-assembly of two different diblock copolymers, many reports are available in the literature.[18−24] For example, Eisenberg et al. prepared polymeric vesicles from a mixture of polystyrene-*b*-poly(acrylic acid) (PS-*b*-PAA) and polystyrene-*b*-poly(4-vinylpridine) (PS-*b*-P4VP).[18,19] The structures of these hybrid vesicles could be tailored by changing the lengths of PAA and P4VP. It was found that the longer P4VP chains segregated to the outer leaf of the vesicle, whereas the shorter PAA chains were distributed in the inner leaf. Apart from hybrid vesicles, polymeric hybrid micelles with stabilized cores and mixed coronas self-assembled from two diblock copolymers have also been reported.[20,22−24] Štìpánek et al. explored the cooperative self-assembly behaviors of mixtures of polystyrene-*b*-poly(methacrylic acid) (PS-*b*-PMA) and polystyrene-*b*-poly(ethylene oxide) (PS-*b*-PEO) in solution.[23] Hybrid polymeric micelles were observed with compact PS cores and mixed PMA/PEO coronas over the whole range of mixture ratios.

In comparison with experimental studies, theoretical work regarding the cooperative self-assembly behaviors of two different diblock copolymers is limited.[25−28] Potemkin et al. developed a theory to predict the thermodynamic stability of hybrid micelles with various morphologies in solutions of AB and BC copolymers in selective solvents within the framework of scaling theory.[25] Both hybrid micelles and ordinary micelles are formed, depending on the incompatibility of soluble blocks A and C. Recently, a hierarchical assembly of a mixture of two different diblock copolymers with a common hydrophobic block but dissimilar hydrophilic blocks was studied by Pitera et al. using coarse-grained molecular dynamics simulations.[26] Their studies indicated that such a mixture can form "patchy" spherical and cylindrical micelles in water. However, most theoretical studies reported so far are limited to micellar structures. Studies on aggregates other than micelles and on aggregate structure change are rather limited.

Real-space self-consistent field theory (SCFT) has emerged as a powerful tool for studying the equilibrium thermodynamic features of polymers.[29−34] This method was extended to investigate the self-assembly behaviors of amphiphilic copolymers in dilute solution.[35−41] Complex micelles and vesicles can be obtained by tailoring the interaction parameters, initial density fluctuation, and polydispersity. This method was also used to study more complex architectural copolymers in dilute solution, such as ABC linear and star triblock copolymers.[39−41] In our previous work, we utilized the SCFT solved in real space to study the aggregate morphologies of amphiphilic graft copolymers and the self-assembly behavior of amphiphilic block copolymer/nanoparticle mixtures in dilute solution.[42,43] The calculation results were in good agreement with the experimental observations. However, most of the SCFT work reported so far

* Corresponding author. Tel.: +86-21-64253370. Fax: +86-21-64253539. E-mail: jplinlab@online.sh.cn.

10.1021/jp809181d CCC: $40.75
Published on Web 01/26/2009

has been performed in two dimensions, and the information provided could be limited.

In this work, three-dimensional real-space self-consistent field theory was used to study the self-assembly of binary mixtures of AB and AC diblock copolymers in dilute solution. For the studied AB and AC diblock copolymers, the A block is insoluble, whereas the B and C blocks are soluble. Two cases were investigated: one in which AB and AC have the same hydrophobic and hydrophilic block lengths and one in which AB and AC have different hydrophobic and hydrophilic block lengths. The effects of the ratio of AB to AC in the mixture and the interaction between the B and C blocks were examined. On the basis of the calculation results, phase diagrams were mapped out to show the influences of the mixture ratio and the interaction between the B and C blocks on the cooperative self-assembly behaviors.

Theoretical Method

We consider a system with volume V, containing n_1 AB diblock copolymers, n_2 AC diblock copolymers, and n_S solvent molecules. Each AB diblock copolymer is composed of N_{A1} and N_B segments, and the total number of segments, N_1, is equal to $N_{A1} + N_B$. For the AC diblock copolymer, the total number of segments, N_2, is equal to $N_{A2} + N_C$. For simplicity, we assume that the two diblock copolymers have the same chain length, i.e., $N_1 = N_2 = N$. The volume fractions of A in copolymers AB and AC are f_{A1} and f_{A2}, respectively, and those of B in copolymer AB and C in copolymer AC are f_B and f_C, respectively ($f_{A1} + f_B = 1, f_{A2} + f_C = 1$). We assume that the mixture is incompressible, with each polymer segment occupying a fixed volume ρ_0^{-1} and each solvent molecule taking the same volume $v_S = \rho_0^{-1}$. The volume fractions of the copolymers AB and AC are c_{AB} and c_{AC}, respectively, and that of the solvent is $c_S = 1 - c_{AB} - c_{AC}$. Furthermore, we assume that the A, B, and C segments have the same statistical length a.

In the SCFT, the pair interactions between different components are determined by a set of effective chemical potential fields $\omega_i(\mathbf{r})$ (i = A, B, C, and S), replacing actual interactions. Hence, the free energy of the AB/AC system is given by

$$\frac{NF}{\rho_0 k_B T V} = -c_{AB}\ln\left(\frac{Q_{AB}}{c_{AB}V}\right) - c_{AC}\ln\left(\frac{Q_{AC}}{c_{AC}V}\right) - c_S N\ln\left(\frac{Q_S}{c_S V}\right) + \frac{1}{V}\int d\mathbf{r}\left\{\frac{1}{2}\sum_{\substack{i,j=A,B,C,S\\ i\neq j}}\chi_{ij}N\phi_i(\mathbf{r})\,\phi_j(\mathbf{r}) - \sum_{i=A,B,C,S}\omega_i(\mathbf{r})\,\phi_i(\mathbf{r}) - \xi(\mathbf{r})\left[1 - \sum_{i=A,B,C,S}\phi_i(\mathbf{r})\right]\right\} \quad (1)$$

where k_B is the Boltzmann constant; T is the temperature; χ_{ij} characterize the Flory−Huggins interaction parameter between species i and j; ξ is the Lagrange multiplier; and $\phi_A(\mathbf{r})$, $\phi_B(\mathbf{r})$, $\phi_C(\mathbf{r})$, and $\phi_S(\mathbf{r})$, which correspond to the density fields, are the local volume fractions of A segments, B segments, C segments, and solvent molecules, respectively. $Q_S = \int d\mathbf{r}\,\exp[-\omega_S(\mathbf{r})/N]$ is the partition function of the solvent in the chemical potential field $\omega_S(\mathbf{r})$. $Q_{AB} = \int d\mathbf{r}\, q_{AB}(\mathbf{r},s)\, q^+_{AB}(\mathbf{r},s)$ is the partition function for a single noninteracting AB diblock copolymer chain subject to fields $\omega_A(\mathbf{r})$ and $\omega_B(\mathbf{r})$. $Q_{AC} = \int d\mathbf{r}\, q_{AC}(\mathbf{r},s)\, q^+_{AC}(\mathbf{r},s)$ is the partition function for a single noninteracting AC diblock copolymer chain subject to fields $\omega_A(\mathbf{r})$ and $\omega_C(\mathbf{r})$. The contour length, s, increases continuously from 0 to 1 as the block changes from one end of the copolymer chain to the other. The spatial coordinate $\mathbf{r}$ is in units of R_g, where $R_g^2 = Na^2/6$. The propagators $q_{AB}(\mathbf{r},s)$ and $q_{AC}(\mathbf{r},s)$ represent the probability of finding segments s at position $\mathbf{r}$, which satisfy the modified diffusion equations

$$\frac{\partial q_{AB}(\mathbf{r},s)}{\partial s} = \nabla^2 q_{AB}(\mathbf{r},s) - \omega_i(\mathbf{r})\, q_{AB}(\mathbf{r},s)$$
$$\omega_i(\mathbf{r}) = \begin{cases}\omega_A(\mathbf{r}) & 0 \le s < f_{A1}\\ \omega_B(\mathbf{r}) & f_{A1} \le s \le 1\end{cases} \quad (2)$$

$$\frac{\partial q_{AC}(\mathbf{r},s)}{\partial s} = \nabla^2 q_{AC}(\mathbf{r},s) - \omega_i(\mathbf{r})\, q_{AC}(\mathbf{r},s)$$
$$\omega_i(\mathbf{r}) = \begin{cases}\omega_A(\mathbf{r}) & 0 \le s < f_{A2}\\ \omega_C(\mathbf{r}) & f_{A2} \le s \le 1\end{cases} \quad (3)$$

subject to the initial conditions $q_{AB}(\mathbf{r},0) = 1$ and $q_{AC}(\mathbf{r},0) = 1$. The backward propagators, $q^+_{AB}(\mathbf{r},s)$ and $q^+_{AC}(\mathbf{r},s)$, satisfy eqs 2 and 3, subject to the initial conditions $q^+_{AB}(\mathbf{r},1) = 1$ and $q^+_{AC}(\mathbf{r},1) = 1$, respectively.

The density of each component is obtained as

$$\phi_A(\mathbf{r}) = \frac{Vc_{AB}}{Q_{AB}}\int_0^{f_{A1}} ds\, q_{AB}(\mathbf{r},s)\, q^+_{AB}(\mathbf{r},s) + \frac{Vc_{AC}}{Q_{AC}}\int_0^{f_{A2}} ds\, q_{AC}(\mathbf{r},s)\, q^+_{AC}(\mathbf{r},s) \quad (4)$$

$$\phi_B(\mathbf{r}) = \frac{Vc_{AB}}{Q_{AB}}\int_{f_{A1}}^{1} ds\, q_{AB}(\mathbf{r},s)\, q^+_{AB}(\mathbf{r},s) \quad (5)$$

$$\phi_C(\mathbf{r}) = \frac{Vc_{AC}}{Q_{AC}}\int_{f_{A2}}^{1} ds\, q_{AC}(\mathbf{r},s)\, q^+_{AC}(\mathbf{r},s) \quad (6)$$

$$\phi_S(\mathbf{r}) = \frac{Vc_S}{Q_S}\exp\left[\frac{-\omega_S(\mathbf{r})}{N}\right] \quad (7)$$

Minimization of the free energy, F, with respect to $\phi_A(\mathbf{r})$, $\phi_B(\mathbf{r})$, $\phi_C(\mathbf{r})$, and $\xi(\mathbf{r})$, leads to the following equations

$$\omega_A(\mathbf{r}) = \chi_{AB}N\phi_B(\mathbf{r}) + \chi_{AC}N\phi_C(\mathbf{r}) + \chi_{AS}N\phi_S(\mathbf{r}) + \xi(\mathbf{r}) \quad (8)$$

$$\omega_B(\mathbf{r}) = \chi_{AB}N\phi_A(\mathbf{r}) + \chi_{BC}N\phi_C(\mathbf{r}) + \chi_{BS}N\phi_S(\mathbf{r}) + \xi(\mathbf{r}) \quad (9)$$

$$\omega_C(\mathbf{r}) = \chi_{AC}N\phi_A(\mathbf{r}) + \chi_{BC}N\phi_B(\mathbf{r}) + \chi_{CS}N\phi_S(\mathbf{r}) + \xi(\mathbf{r}) \quad (10)$$

$$\omega_S(\mathbf{r}) = \chi_{AS}N\phi_A(\mathbf{r}) + \chi_{BS}N\phi_B(\mathbf{r}) + \chi_{CS}N\phi_C(\mathbf{r}) + \xi(\mathbf{r}) \quad (11)$$

$$\phi_A(\mathbf{r}) + \phi_B(\mathbf{r}) + \phi_C(\mathbf{r}) + \phi_S(\mathbf{r}) = 1 \quad (12)$$

We solved eqs 4−12 directly in real space by using a combinatorial screening algorithm proposed by Drolet and Fredrickson.[44−47] The initial values of the density fields $\phi_i(\mathbf{r})$ were assumed to satisfy the Gaussian distributions[35]

$$\langle \phi_i(\mathbf{r}) - \varphi_i \rangle = 0 \quad (13)$$

$$\langle [\phi_i(\mathbf{r}) - \varphi_i][\phi_j(\mathbf{r}') - \varphi_j] \rangle = \beta \varphi_i \varphi_j \delta_{ij} \delta(\mathbf{r} - \mathbf{r}') \quad (14)$$

Here, β characterizes the amplitude of initial density fluctuation, and φ_i (i = A, B, C, and S) represents the volume fractions of block A, block B, block C, and solvent, respectively, in solution. These diffusion equations (eqs 2 and 3) were solved with the Baker−Hansdorff operator splitting formula proposed by Rasmussen et al.,[48,49] which has a higher stability and accuracy than other methods for the same spatial discretization. The right-hand sides of eqs 4−7 were evaluated to obtain new expressions for the volume fractions, $\phi_i(\mathbf{r})$, of species i. To ensure the incompressibility of the system, the effective pressure field, $\xi(\mathbf{r})$, was obtained by solving eqs 8−12.[35] The potential fields, $\omega_i(\mathbf{r})$, and pressure field, $\xi(\mathbf{r})$, were updated using eqs 8−11 by means of a two-step Anderson mixing scheme.[50]

All simulations were performed in three dimensions on a 48 × 48 × 48 lattice with periodic boundary conditions. The contour step size was set to 0.01. It is noted that the resulting aggregate morphologies depend on the amplitude of the initial density fluctuation. As a result, the same initial density fluctuation amplitude ($\beta = 10^{-3}$) was used in our simulations to ensure that the obtained morphologies were not affected by the initial fluctuation, as is done in the literature on the self-assembly of copolymers in dilute solution.[35,36,39,40] Following Fredrickson's method of real-space implementation of SCFT,[44−46] which has been found to be an efficient way to tackle the problem of self-assembled complex structures in dilute copolymer solution,[35,36,39,40] we started from a Gaussian distribution initial density profile and let the system evolve to equilibrium in three-dimensional lattice space. To check the dependence of the obtained structure on the initial state, different random numbers were used to generate Gaussian distributions at a given initial density fluctuation amplitude.[45,47] In the calculations, simulations starting from a homogeneous copolymer solution were repeated 10−20 times using different random initial states and different random numbers to ensure that the observed phenomena were not accidental.

Results and Discussion

In this work, the concentration of copolymers was set to $c_{AB} + c_{AC} = 0.1$ to ensure that the copolymers were in dilute solution. The chain lengths of the two block copolymers were assumed to be $N_1 = N_2 = N = 20$. Block A was assumed to be hydrophobic, and the interaction parameter between block A and solvent was fixed at $\chi_{AS}N = 34.0$. The other two blocks, B and C, were assumed to be hydrophilic, and $\chi_{BS}N$ and $\chi_{CS}N$ were taken to be −2.0. For the sake of simplicity, the interaction parameters between blocks A and B in copolymer AB and between blocks A and C in copolymer AC were fixed at $\chi_{AB}N = \chi_{AC}N = 9.0$. Two cases were investigated in the present work: one in which AB and AC have the same hydrophobic and hydrophilic block lengths and one in which AB and AC have different hydrophobic and hydrophilic block lengths.

A. Cooperative Self-Assembly of AB and AC Block Copolymers with Same Hydrophobic and Hydrophilic Block Lengths. In this subsection, the lengths of the hydrophobic blocks are considered to be the same for both copolymers. The volume fractions of block A in both AB and AC (f_{A1}, f_{A2}) were set to 0.83. Figure 1 shows the morphology transformations of the formed aggregates with increasing repulsion between blocks B and C at $c_{AB} = 0.05$ (c_{AB} is the volume fraction of copolymer AB in solution). When $\chi_{BC}N$ is low, the interaction between blocks B and C is weak, and vesicles are formed (Figure 1a). As $\chi_{BC}N$ increases, the incompatibility between hydrophilic blocks B and C becomes relatively larger, and spherical micelles appear. Consequently, the aggregate morphology transforms from vesicles to a mixture of vesicles and micelles (Figure 1b,c).

As stated above, the morphological transition from vesicles to micelles can be triggered by increasing incompatibility between the hydrophilic blocks B and C. When the interaction between blocks B and C is weaker, the self-assembly of the AB/AC copolymer mixture can be considered as the self-assembly of neat AB or AC copolymers because the AB and AC copolymers have same properties in solution. Under such circumstances, vesicles are formed. As the interaction between different hydrophilic blocks becomes stronger, the interaction energy in the inner leaf of the vesicles increases substantially. To depress this effect, the hydrophilic blocks transfer from the inner leaf to the outer leaf of the vesicle in order to reduce their interfaces. As more hydrophilic blocks transfer to the outer leaf, the vesicle aggregates cannot be sustained. Consequently, the transition from vesicles to a mixture of vesicles and micelles takes place.

To obtain detailed structural information regarding the hybrid aggregates in the morphology transformation, the density distributions of the respective components of the two copolymers are plotted for vesicles at different values of $\chi_{BC}N$ in Figure 2. The curves of the volume fraction of hydrophobic blocks A_1 and A_2 or hydrophilic blocks B and C are indistinguishable. This is ascribed to the fact that the AB and AC diblock copolymers have the same chain length. Figure 2a shows the density distribution profile for vesicles at $\chi_{BC}N = 0.0$. The profile of ϕ_A exhibits a bimodal feature, i.e., the hydrophobic A (including A_1 and A_2) blocks form the wall of the vesicle. The inner and outer leaves of the vesicles are composed of hydrophilic blocks B and C. Figure 2b shows the density distribution profile for the aggregates at $\chi_{BC}N = 30.0$. The density distribution of the hydrophobic blocks has a quasibimodal feature similar to that of the vesicles, as shown in Figure 2a. However, the distribution of hydrophilic blocks is different from that of the vesicles. The maximum local volume fraction of hydrophilic blocks appears in the center of the aggregate rather than in the inner surface. This type of aggregate is termed a quasivesicle.[36,51]

To provide an overview of the effects of the mixture composition and the repulsive interaction between blocks B and C on the aggregation behavior, we plot the aggregate morphology stability regions for AB/AC mixtures in c_{AB} versus $\chi_{BC}N$ space. The phase diagram is shown in Figure 3. Each point in the phase diagram corresponds to a simulation result, and lines are drawn to identify the resulting phase boundaries. The phase diagram is divided into two characteristic zones: vesicles (**V**) and a mixture of quasivesicles and micelles (**QV** + **M**). The phase diagram is symmetric about $c_{AB} = 0.05$. The **V**/(**QV** + **M**) phase boundaries shift toward higher values of $\chi_{BC}N$ as c_{AB} becomes smaller or greater. The lowest value of $\chi_{BC}N$ for the transition between **V** and **QV** + **M** is shown at $c_{AB} = 0.05$ due to the fact that the actual interaction between hydrophilic blocks B and C is strongest when the volume fractions of copolymers AB and AC are comparable. When the volume fractions of copolymers AB and AC become much different, the actual interaction between hydrophilic blocks B and C is reduced, resulting in an upward shift of the phase boundaries.

It should be emphasized that, because of the large parameter space and also for the simplicity of the studies, only one specific

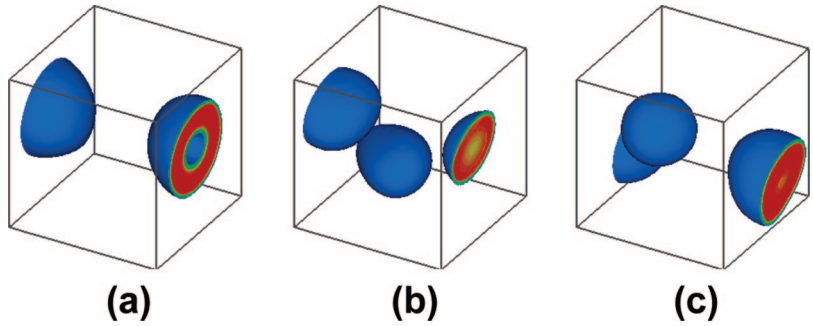

Figure 1. Aggregate morphologies self-assembled from AB/AC diblock copolymers in dilute solution with an increase in interaction strength, $\chi_{BC}N$, between hydrophilic blocks B and C at $c_{AB} = 0.05$: (a) $\chi_{BC}N = 0.0$, (b) $\chi_{BC}N = 15.0$, and (c) $\chi_{BC}N = 30.0$. The red and blue colors indicate the hydrophobic A blocks and the coexistence of hydrophilic B and C blocks, respectively. The solvent molecules are not illustrated for clarity.

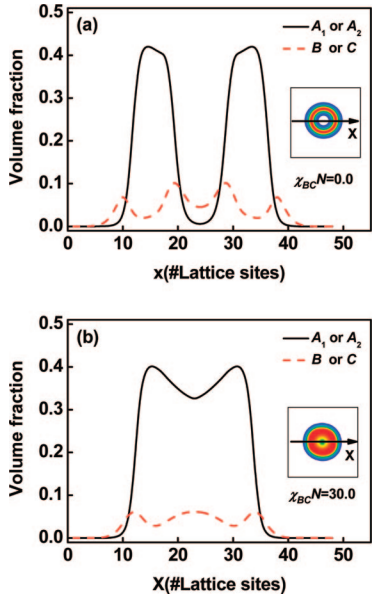

Figure 2. Density distribution profiles of hydrophobic blocks ϕ_{A1} (or ϕ_{A2}) and hydrophilic blocks ϕ_B (or ϕ_C) on a cross section of aggregate marked with an arrow in the inset at $c_{AB} = 0.05$: (a) vesicle, $\chi_{BC}N = 0.0$; (b) quasivesicle, $\chi_{BC}N = 30.0$. The insets are two-dimensional distributions of hydrophobic A blocks, where the density of A blocks increases as the color changes from blue to red.

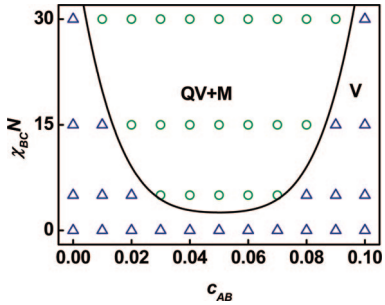

Figure 3. Aggregate morphology stability regions of AB/AC diblock copolymer solutions plotted as functions of the interaction strength, $\chi_{BC}N$, between blocks B and C and the AB diblock copolymer volume fraction c_{AB}. The notations **V** and **QV + M** represent vesicles and a mixture of quasivesicles and micelles, respectively. Each point in the phase diagram corresponds to a simulation result, and lines are drawn to identify the resulting phase boundaries.

total copolymer concentration was considered in the present work ($c_{AB} + c_{AC} = 0.1$). The concentration was chosen to be greater than the critical micelle concentration and smaller than the overlap critical concentration to ensure that the systems were dilute solutions. However, variations of the copolymer concentration have an effect on the morphology of the self-assemblies. For example, for the self-assembly of AB and AC copolymers with same hydrophobic and hydrophilic block lengths, at $c_{AB}/c_{AC} = 5/5$, $\chi_{BC}N = 15.0$, and $c_{AB} + c_{AC} = 0.10$, a mixture of micelles and quasivesicles is observed. However, when the total polymer concentration is decreased to $c_{AB} + c_{AC} = 0.07$, the aggregate morphology transforms to quasivesicles. When the total polymer concentration is increased to $c_{AB} + c_{AC} = 0.15$, the aggregate morphology changes to a mixture of spherical and cylindrical micelles.

B. Cooperative Self-Assembly of AB and AC Block Copolymers with Different Hydrophobic and Hydrophilic Block Lengths. In this section, the chain length of hydrophobic block A_1 in copolymer AB is considered to be longer than that of hydrophobic block A_2 in copolymer AC, whereas the chain length of hydrophilic block B is shorter than that of hydrophilic block C. In the calculations, the composition of the A_1 block was set to $f_{A1} = 0.83$, and that of the A_2 block was set to $f_{A2} = 0.70$.

Figure 4 shows the morphology changes of the hybrid aggregates with increasing volume fraction of copolymer AB, c_{AB}. Spherical micelles are observed for AC diblock copolymer and for the mixtures with lower contents of copolymer copolymer AB (Figure 4a,b). As c_{AB} increases, a morphological transition from spherical micelles to a mixture of spherical and cylindrical micelles takes place, which is shown in Figure 4c. With further increasing c_{AB}, quasivesicles appear (Figure 4d). Vesicles and micelles form when copolymer AB becomes the major part of the mixture (Figure 4e). When the volume fraction of copolymer AB is close to 0.10, vesicles are the only morphology observed (Figure 4f). At $c_{AB} = 0.10$, vesicles are assembled only from copolymer AB, as no copolymer AC is present.

The density distribution profiles of hydrophobic blocks A_1 and A_2 and hydrophilic blocks B and C blocks were analyzed for the aggregates at different volume fractions of AB diblock copolymers, c_{AB}. The results are presented in Figure 5. Figure 5a shows the distribution profiles of spherical micelles at $c_{AB} = 0.01$. The hydrophobic A_1 and A_2 blocks form the core, and the hydrophilic B and C blocks form the corona. When c_{AB} increases, the content of shorter hydrophilic blocks from copolymer AB increases. As shown in Figure 5b, the shorter hydrophobic blocks A_2 in the core tend to be located close to the hydrophobic−hydrophilic interface, whereas the longer A_1 blocks extend to the interior of the core. Meanwhile, the shorter hydrophilic blocks B start to enter the core, and the C blocks still remain in the corona. As c_{AB} increases further to 0.065 (see Figure 5c), more shorter hydrophilic B blocks localize in the core, and the hydrophobic A_1 and A_2 blocks are both excluded from the interior of the core. Because the volume

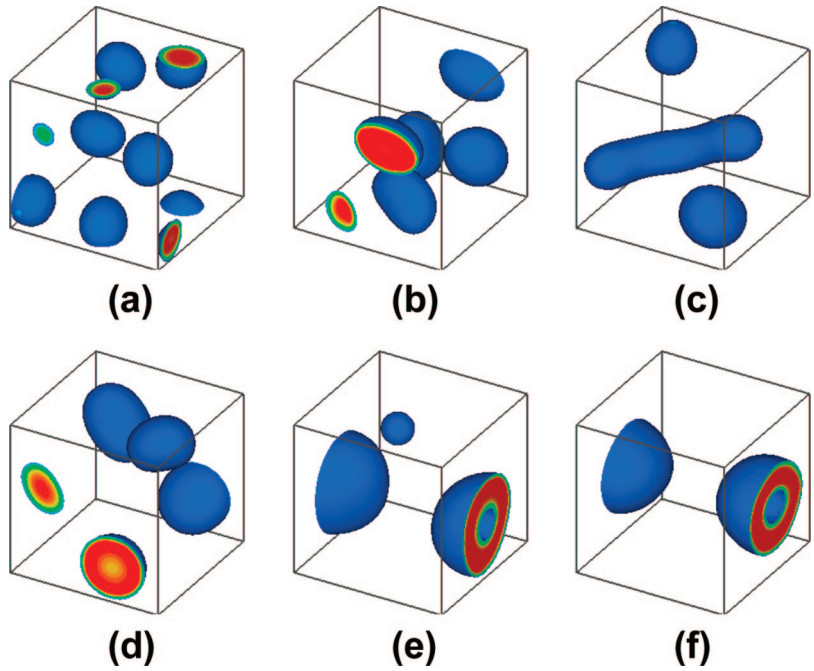

Figure 4. Aggregate morphologies self-assembled from AB/AC diblock copolymers in dilute solution with an increase in the volume fraction of copolymer AB c_{AB} at $\chi_{BC}N = 0.0$: (a) $c_{AB} = 0.01$, (b) $c_{AB} = 0.02$, (c) $c_{AB} = 0.04$, (d) $c_{AB} = 0.065$, (e) $c_{AB} = 0.078$, and (f) $c_{AB} = 0.09$. The red and blue colors indicate the hydrophobic A blocks and the coexistence of hydrophilic B and C blocks, respectively. The solvent molecules are not illustrated for clarity.

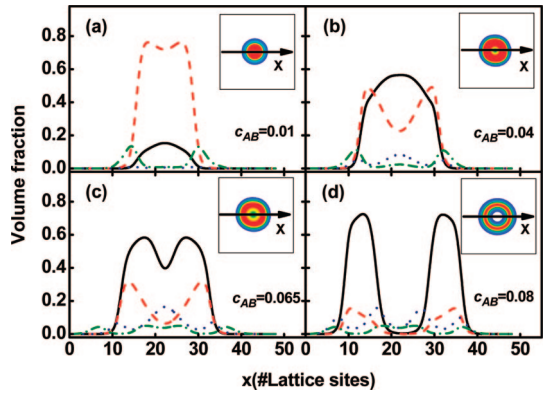

Figure 5. Density distribution profiles of hydrophobic A_1 blocks (black solid line), hydrophobic A_2 blocks (red dashed line), hydrophilic B blocks (navy dotted line), and hydrophilic C blocks (olive dash-dotted line) on a cross section of aggregate marked with an arrow in the inset at $\chi_{BC}N = 0.0$: (a) spherical micelle, $c_{AB} = 0.01$; (b) quasivesicle, $c_{AB} = 0.04$; (c) quasivesicle, $c_{AB} = 0.065$; and (d) vesicle, $c_{AB} = 0.08$. The insets are two-dimensional distributions of hydrophobic A blocks, where the density of A blocks increases as the color changes from blue to red.

fraction of the interior hydrophilic blocks becomes larger, the longer hydrophilic blocks C can then enter the core. Consequently, the micelles are reorganized into quasivesicles. Because of the increased number of hydrophilic blocks in the interior, more solvent molecules are absorbed into the quasivesicle and swell the hydrophilic copolymer blocks in the center of the quasivesicle. A complete vesicle is built when c_{AB} increases to 0.08 (see Figure 5d). In the formed vesicles, the shorter hydrophilic blocks B mainly are present in the inner leaf.

The morphological changes of the aggregates with increasng repulsion of blocks B and C are shown in Figure 6. In the calculations, the volume fraction of block copolymer AB, c_{AB}, is fixed at 0.08. When $\chi_{BC}N = 0$, vesicles are observed (Figure 6a). As $\chi_{BC}N$ increases to 15, a transition from the vesicles to micelles occurs, and a mixture of vesicles and spherical micelles is found, as shown in Figure 6b. With further increasing $\chi_{BC}N$, a mixture of quasivesicles and spherical micelles forms (Figure 6c).

The density distributions of the respective components are plotted for vesicles and quasivesicles at $c_{AB} = 0.08$ as a function of $\chi_{BC}N$ (Figure 7). As $\chi_{BC}N$ increases from 0 to 30.0, the density distributions of the hydrophobic blocks change from the typical bimodal feature of vesicles (Figure 7a) to a quasibimodal feature of quasivesicles (Figure 7b). Unlike the cases in Figure 2, there is segregation of the blocks in both the vesicles and quasivesicles. For the vesicles (Figure 7a), the longer hydrophobic blocks A_1 in the wall tend to be located close to the inner leaf, whereas the shorter A_2 blocks in the wall tend to be distributed close to the outer leaf. At $\chi_{BC}N = 0$, the density distributions of B and C blocks are typical vesicle distributions with a bilayer comprising inner and outer leafs. Compared to the C blocks, the shorter B blocks prefer to reside in the inner leaf (see Figure 7a). As $\chi_{BC}N$ increases, the density distribution becomes unimodal, characteristic of quasivesicles (see Figure 7b). Meanwhile, the volume fraction of C blocks in the interior decreases sharply, implying that the longer hydrophilic C blocks move to the outer leaf as $\chi_{BC}N$ increases.

As shown in Figures 6 and 7, the $\mathbf{V} \rightarrow (\mathbf{V} + \mathbf{M}) \rightarrow (\mathbf{QV} + \mathbf{M})$ morphology transitions at $c_{AB} = 0.08$ exhibit a distinctive feature with respect to the distribution of hydrophilic blocks B and C. The shorter hydrophilic blocks have a preference to remain in the inner leaf of vesicles or quasivesicles. To further rationalize this process, a cartoon is presented in Figure 8. When $\chi_{BC}N$ is small, a vesicle forms (Figure 8a). As $\chi_{BC}N$ increases, blocks B and C become more incompatible, especially in the narrow inner leaf of vesicle. A transfer of blocks B and C to the outer leaf can alleviate the repulsion between them. Consequently, the vesicles cannot be sustained, and quasivesicles and spherical micelles appear (Figure 8b,c). In the quasivesicles, the inner space becomes much narrower than that in the vesicles. It is enthalpically unfavorable for the longer C blocks to reside in this narrower interior. Therefore, the C blocks prefer to reside

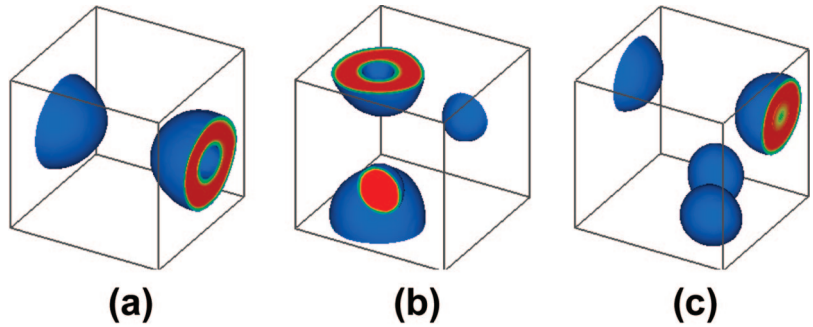

Figure 6. Aggregate morphologies self-assembled from AB/AC diblock copolymers in dilute solution with an increase interaction strength, $\chi_{BC}N$, between B and C blocks at $c_{AB} = 0.08$: (a) $\chi_{BC}N = 0.0$, (b) $\chi_{BC}N = 15.0$, and (c) $\chi_{BC}N = 30.0$. The red and blue colors indicate the hydrophobic A blocks and the coexistence of hydrophilic B and C blocks, respectively. The solvent molecules are not illustrated for clarity.

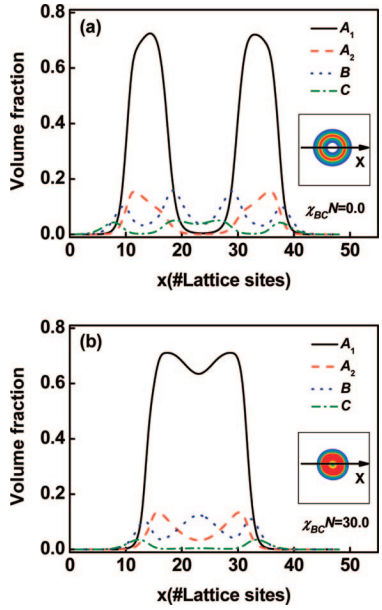

Figure 7. Density distribution profiles of hydrophobic A_1 blocks, hydrophobic A_2 block, hydrophilic B blocks, and hydrophilic C blocks on a cross section of aggregate marked with an arrow in the inset at $c_{AB} = 0.08$: (a) vesicle, $\chi_{BC}N = 0.0$; (b) quasivesicle, $\chi_{BC}N = 30.0$. The insets are two-dimensional distributions of hydrophobic A blocks, where the density of A blocks increases as the color changes from blue to red.

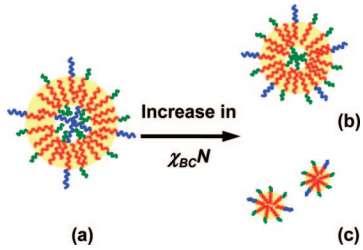

Figure 8. Schematic representations of (a) vesicles, (b) quasivesicles, and spherical micelles for the AB/AC diblock copolymer system. The red lines, blue lines, and olive lines denote the hydrophobic A blocks, hydrophilic B blocks, and hydrophilic C blocks, respectively. The solvent molecules are not illustrated for clarity.

in the outer leaf, and the B blocks remain in the interior at higher values of $\chi_{BC}N$, as shown in Figure 8b.

Based on the calculations, we determined the morphology stability regions as functions of c_{AB} and $\chi_{BC}N$, as shown in Figure 9. Five characteristic zones are included in the phase diagram: vesicles (**V**), mixture of vesicles and spherical micelles (**V** + **M**), mixture of quasivesicles and spherical micelles (**QV** + **M**), mixture of cylindrical and spherical micelles (**C** + **M**),

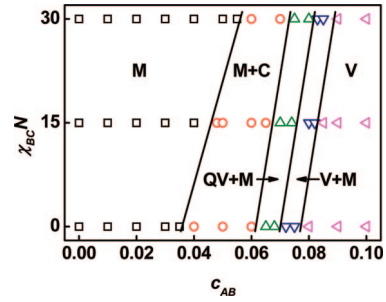

Figure 9. Aggregate morphology stability regions of AB/AC diblock copolymer solution plotted as functions of the interaction strength, $\chi_{BC}N$, between blocks B and C and the volume fraction of AB diblock copolymer, c_{AB}. The notations **M**, **M** + **C**, **QV** + **M**, **V** + **M**, and **V** represent spherical micelles, a mixture of spherical and cylindrical micelles, a mixture of quasivesicles and spherical micelles, a mixture of vesicles and spherical micelles, and vesicles, respectively.

and spherical micelles (**M**). As c_{AB} increases, transitions take place in the order **M** → (**C** + **M**) → (**QV** + **M**) → (**V** + **M**) → **V**. With increasing value of $\chi_{BC}N$, the phase boundaries shift to higher values of c_{AB}. In comparison with Figure 3, this phase diagram is no longer symmetric, because the hydrophobic and hydrophilic block lengths in copolymers AB and AC are different. However, the transition from a mixture of micelles and quasivesicles to vesicles is observed in the two phase diagrams with decreasing $\chi_{BC}N$ at an appropriate value of c_{AB}. This indicates that the interactions of different blocks in the two copolymers have an important effect on the self-assembly of the binary mixture.

In the present work, we considered only two cases of block-length asymmetry for simplicity. One is that copolymers AB and AC have the same hydrophobic and hydrophilic block lengths ($f_{A1} = f_{A2} = 0.83$); the other is that copolymers AB and AC have different hydrophobic and hydrophilic block lengths ($f_{A1} = 0.83$ and $f_{A2} = 0.70$). However, the variation of block-length asymmetry has an effect on the morphology of the self-assemblies. For example, for the self-assembly of copolymers AB and AC with different hydrophobic and hydrophilic block lengths, at $c_{AB}/c_{AC} = 7/3$ and $\chi_{BC}N = 0$, a mixture of micelles and vesicles is observed at $f_{A2} = 0.70$. When f_{A2} is changed to 0.59, a mixture of micelles and quasivesicles appears.

Some experimental results on cooperative self-assembly are available in the literature for comparison with the theoretical predications. For example, a spontaneous micelle → vesicle transition has been experimentally observed in an aqueous solution containing two amphiphilic surfactants, lecithin and bile salt.[52,53] Lecithin alone forms vesicles with low curvature, whereas bile salt forms highly curved spherical micelles. The morphological transition of the aggregates as a function of bile

salt content was investigated. For the mixed system, transitions from micelles to long cylindrical micelles and then to vesicles were observed, as the content of lecithin increased. In our SCFT calculations (Figure 9), at certain values of $\chi_{BC}N$, with an increase in c_{AB}, **M** → (**C** + **M**) → (**QV** + **M**) → (**V** + **M**) → **V** transitions are demonstrated. The general features of the morphological transitions predicted by SCFT are consistent with the experimental observations, even though the model of block copolymers has a well-defined architecture.

Uddin et al. studied the aggregation behavior of mixtures of poly(oxyethylene)-*b*-poly(dimethyl siloxane) ($Si_{25}C_3EO_{51.6}$) copolymer and nonionic surfactant [penta(ethylene glycol) monododecyl ether, $C_{12}EO_5$] in water.[54] Hybrid micelles with a core−shell structure were observed. It was proposed that the shorter hydrophobic blocks of the surfactant in the core were close to the hydrophobic−hydrophilic interfaces, whereas the longer hydrophobic blocks of poly(oxyethylene)-*b*-poly(dimethyl siloxane) extended into the interior of the core. In the corona, the shorter EO_5 blocks localized around the interfaces, whereas the longer $EO_{51.6}$ blocks extended outward to form a brush. In the present work, we calculated the aggregate structure self-assembled from a mixture of AB and AC block copolymers with different hydrophobic and hydrophilic block lengths. Figure 5a shows the distribution of each block in mixed micelles for $f_C > f_B$. The longer hydrophobic chains A_1 are found primarily in the interior of the core, whereas the shorter A_2 chains are primarily found closer to the hydrophobic−hydrophilic interface. In the corona, the longer C blocks extend to the outside, and conversely, the shorter B blocks remain close to the core−shell interface. Our SCFT results agree well with the experimental observations.

Pispas et al. recently investigated the self-assembly behavior of mixtures of poly(isoprene-*b*-ethylene oxide) (IEO) amphiphilic block copolymers and didodecyldimethylammonium bromide (DDAB) surfactant in aqueous solution.[55] Micelles were observed in IEO solutions, whereas vesicles were found in DDAB solutions. Hybrid aggregates were found when IEO and DDAB were mixed in aqueous solution. At higher temperatures, hybrid vesicles were produced. With decreasing temperature, the vesicles shrank, and the size decreased. A further decrease in temperature led to disruption of the vesicles and the formation of micelles. In our calculations, we found that the value of $\chi_{BC}N$ plays a crucial role in morphology transitions. An increase in $\chi_{BC}N$ corresponds to a decrease in temperature in experiments.[56] As shown in Figure 8, with increasing $\chi_{BC}N$, the morphologies undergo a transition from vesicles to a mixture of quasivesicles and micelles. The general features of the SCFT predictions are in line with the experimental observations.

Eisenberg et al. observed a chain segregation phenomenon in vesicles self-assembled from mixtures of two polystyrene-*b*-poly(acrylic acid) (PS-*b*-PAA) samples with different PAA lengths by using a fluorescently labeled diblock of the short PAA chain.[19,57,58] They found that, under appropriate conditions, the short PAA chains mainly segregated to the inner leaf. The inner leaf contained a higher content of short PAA chains than of longer PAA chains. In our theoretical predictions, chains with different lengths in hybrid vesicles show chain segregation. The results presented in Figure 5d demonstrate that the shorter hydrophilic B blocks mostly remain in the inner leaf and their volume fraction in the interior is higher than that of C blocks in the inner leaf (in Figure 5d, $\chi_{BC}N = 0$, which means that B and C are the same). Such chain segregation behavior agrees with Eisenberg et al.'s experimental observations of hybrid vesicles formed by mixtures of diblock copolymers with different lengths.

The self-consistent field theory (SCFT), which originated from the field theoretical approach of Edwards, has emerged as a powerful tool for studying the equilibrium thermodynamic features of polymers.[45,59−61] Recently, this theory was successfully extended to investigate the aggregation behavior of amphiphilic copolymers in dilute solution.[35−43] In this work, we presented a systemic study of cooperative self-assembly behavior of a mixture of two diblock copolymers using SCFT. The theoretical calculations show a qualitative agreement with the existing experimental results. However, it should be noted that the neglect of thermal fluctuations in the formalism of mean-field theory could cause some drawbacks in the simulations. The effects of fluctuations could become important for solutions, especially dilute and semidilute solutions.[62] The phase boundaries of aggregate morphology stability regions in mixed solutions might exhibit some degree of shifts when fluctuations are considered, but the mean-field theory is able to capture the essential features of the self-assembled systems, such as the transitions of the aggregate morphologies and distribution profiles of different blocks.

Conclusions

We applied the real-space SCFT to study the self-assembly behaviors of AB and AC diblock copolymer mixtures in dilute solution. Cooperative self-association of the mixture takes place. The morphologies of the formed aggregates depend on the ratio of AB to AC and the interaction between hydrophilic blocks B and C. For AB and AC having the same hydrophobic and hydrophilic block lengths, **V** → (**QV** + **M**) → **V** transitions take place with increasing content of copolymer AB in the mixtures. For AB/AC mixtures with different hydrophobic and hydrophilic block lengths, **M** → (**C** + **M**) → (**QV** + **M**) → (**V** + **M**) → **V** transitions are found as the content of copolymer AB increases. The theoretical results were compared with some existing experimental observations, and good qualitative agreement was found. The results gained through SCFT analysis suggest that hybrid aggregates can be obtained through cooperative self-assembly of two amphiphilic block copolymers. The microstructures of the hybrid aggregates can be tuned by the mixture ratio of the two copolymers and the interactions between polymer chains. In addition, chain segregation takes place in the hybrid aggregates.

Acknowledgment. This work was supported by the National Natural Science Foundation of China (50673026, 20574018). Support from the Doctoral Foundation of the Education Ministry of China (Grant 20050251008) and Projects of Shanghai Municipality (06SU07002, 082231, and B502) is also appreciated.

References and Notes

(1) van Hest, J. C. M.; Delnoye, D. A. P.; Baars, M. W. P. L.; van Genderen, M. H. P.; Meijer, E. W. *Science* **1995**, *268*, 1592.
(2) Meier, W. *Chem. Soc. Rev.* **2000**, *29*, 295.
(3) Chouchair, A.; Eisenberg, A. *Eur. Phys. J. E* **2003**, *10*, 37.
(4) Antonietti, M.; Förster, S. *Adv. Mater.* **2003**, *15*, 1323.
(5) Jain, S.; Bates, F. S. *Science* **2003**, *300*, 460.
(6) Geng, Y.; Ahmed, F.; Bhasin, N.; Discher, D. E. *J. Phys. Chem. B* **2005**, *109*, 3772.
(7) Harada, A.; Kataoka, K. *Prog. Polym. Sci.* **2006**, *31*, 949.
(8) Discher, D. E.; Eisenberg, A. *Science* **2002**, *297*, 967.
(9) Hadjichristidis, N.; Pispas, S.; Floudas, G. A. *Block Copolymers: Synthetic Strategies, Physical Properties, and Applications*; John Wiley & Sons: New York, 2002.
(10) Riess, G. *Prog. Polym. Sci.* **2003**, *28*, 1107.

(11) Wang, X.; Hall, J. E.; Warren, S.; Krom, J.; Magistrelli, J. M.; Rackaitis, M.; Bohm, G. G. A. *Macromolecules* **2007**, *40*, 499.
(12) Chow, E. K.; Pierstorff, E.; Cheng, G.; Ho, D. *ACS Nano* **2008**, *2*, 33.
(13) Kwon, G. S.; Naito, M.; Yokoyama, M.; Okano, T.; Sakurai, Y.; Kataoka, K. *Pharm. Res.* **1995**, *12*, 92.
(14) Kataoka, K.; Kwon, G. S.; Yokoyama, M.; Okano, T.; Sakurai, Y. *J. Controlled Release* **1993**, *24*, 119.
(15) Harada, A.; Kataoka, K. *Macromolecules* **1995**, *28*, 5294.
(16) Lin, J.; Zhang, S.; Chen, T.; Lin, S.; Jin, H. *Int. J. Pharm.* **2007**, *336*, 49.
(17) Lin, J.; Zhu, J.; Chen, T.; Lin, S.; Cai, C.; Zhang, L.; Zhuang, Y.; Wang, X. *Biomaterials* **2009**, *30*, 108.
(18) Luo, L.; Eisenberg, A. *Angew. Chem., Int. Ed.* **2002**, *41*, 1001.
(19) Luo, L.; Eisenberg, A. *Langmuir* **2001**, *17*, 6804.
(20) Hu, J.; Liu, G. *Macromolecules* **2005**, *38*, 8058.
(21) Yan, X.; Liu, G.; Hu, J.; Willson, C. G. *Macromolecules* **2006**, *39*, 1906.
(22) Li, G.; Shi, L.; Ma, R.; An, Y.; Huang, N. *Angew. Chem., Int. Ed.* **2006**, *45*, 4959.
(23) Štìpánek, M.; Podhájecká, K.; Tesaøová, E.; Procházka, K.; Tuzar, Z.; Brown, W. *Langmuir* **2001**, *17*, 4240.
(24) Hui, T.; Chen, D.; Jiang, M. *Macromolecules* **2005**, *38*, 5834.
(25) Palyulin, V. V.; Potemkin, I. I. *Macromolecules* **2008**, *41*, 4459.
(26) Srinivas, G.; Pitera, J. W. *Nano Lett.* **2008**, *8*, 611.
(27) Sens, P.; Marques, C. M.; Joanny, J.-F. *Macromolecules* **1996**, *29*, 4880.
(28) Palmer, B. J.; Liu, J.; Virden, J. *Langmuir* **1999**, *15*, 7426.
(29) Ye, X.; Shi, T.; Lu, Z.; Zhang, C.; Sun, Z.; An, L. *Macromolecules* **2005**, *38*, 8853.
(30) Ye, X.; Yu, X.; Sun, Z.; An, L. *J. Phys. Chem. B* **2006**, *110*, 12042.
(31) Kou, D.; Jiang, Y.; Liang, H. *J. Phys. Chem. B* **2006**, *110*, 23557.
(32) Chen, P.; Liang, H.; Shi, A.-C. *Macromolecules* **2007**, *40*, 7329.
(33) Zhang, L.; Lin, J.; Lin, S. *J. Phys. Chem. B* **2007**, *111*, 351.
(34) Wang, L.; Zhang, L.; Lin, J. *J. Chem. Phys.* **2008**, *129*, 114905.
(35) He, X.; Liang, H.; Huang, L.; Pan, C. *J. Phys. Chem. B* **2004**, *108*, 1731.
(36) Jiang, Y.; Chen, T.; Ye, F.; Liang, H.; Shi, A.-C. *Macromolecules* **2005**, *38*, 6710.
(37) Zhu, J.; Jiang, Y.; Liang, H.; Jiang, W. *J. Phys. Chem. B* **2005**, *109*, 8619.
(38) Jiang, Y.; Zhu, J.; Jiang, W.; Liang, H. *J. Phys. Chem. B* **2005**, *109*, 21549.
(39) Wang, R.; Tang, P.; Qiu, F.; Yang, Y. *J. Phys. Chem. B* **2005**, *109*, 17120.
(40) Li, X.; Tang, P.; Qiu, F.; Zhang, H.; Yang, Y. *J. Phys. Chem. B* **2006**, *110*, 2024.
(41) Ma, J. W.; Li, X.; Tang, P.; Yang, Y. *J. Phys. Chem. B* **2007**, *111*, 1552.
(42) Zhang, L.; Lin, J.; Lin, S. *J. Phys. Chem. B* **2007**, *111*, 9209.
(43) Zhang, L.; Lin, J.; Lin, S. *Macromolecules* **2007**, *40*, 5582.
(44) Drolet, F.; Fredrickson, G. H. *Macromolecules* **2001**, *34*, 5317.
(45) Drolet, F.; Fredrickson, G. H. *Phys. Rev. Lett.* **1999**, *83*, 4317.
(46) Ganesan, V.; Fredrickson, G. H. *Europhys. Lett.* **2001**, *55*, 814.
(47) Fredrickson, G. H.; Ganesan, V.; Drolet, F. *Macromolecules* **2002**, *35*, 16.
(48) Tzeremes, G.; Rasmussen, K. Ø.; Lookman, T.; Saxena, A. *Phys. Rev. E* **2002**, *65*, 041806.
(49) Rasmussen, K. Ø.; Kalosakas, G. *J. Polym. Sci. B: Polym. Phys.* **2002**, *40*, 1777.
(50) Eyert, V. *J. Comput. Phys.* **1996**, *124*, 271.
(51) Olla, P. *Physica A* **2000**, *278*, 87.
(52) Egelhaaf, S. U.; Schurtenberger, P. *J. Phys. Chem.* **1994**, *98*, 8560.
(53) Long, M. A.; Kaler, E. W.; Lee, S. P. *Biophys. J.* **1994**, *67*, 1733.
(54) Kunieda, H.; Uddin, M. H.; Furukawa, H.; Harashima, A. *Macromolecules* **2001**, *34*, 9093.
(55) Pispas, S.; Sarantopoulou, E. *Langmuir* **2007**, *23*, 7484.
(56) Lodge, T. P.; Pan, C.; Jin, X.; Liu, Z.; Zhao, J.; Maurer, W. W.; Bates, F. S. *J. Polym. Sci. B: Polym. Phys.* **1995**, *33*, 2289.
(57) Terreau, O.; Luo, L.; Eisenberg, A. *Langmuir* **2003**, *19*, 5601.
(58) Soo, P. L.; Eisenberg, A. *J. Polym. Sci. B: Polym. Phys.* **2004**, *42*, 923.
(59) Matsen, M. W.; Schick, M. *Phys. Rev. Lett.* **1994**, *72*, 2660.
(60) Matsen, M. W.; Thompsom, R. B. *J. Chem. Phys.* **1999**, *111*, 7139.
(61) Matsen, M. W. *J. Chem. Phys.* **2000**, *113*, 5539.
(62) De Gennes. P. G. *Scaling Concepts in Polymer Physics*; Cornell University Press: Ithaca, NY, 1979.

JP809181D